

Few-shot Fine-grained Image Classification via Multi-Frequency Neighborhood and Double-cross Modulation

Hegui Zhu, Zhan Gao, Jiayi Wang, Yange Zhou, Chengqing Li.

Abstract—Traditional fine-grained image classification typically relies on large-scale training samples with annotated ground-truth. However, some sub-categories may have few available samples in real-world applications. In this paper, we propose a novel few-shot fine-grained image classification network (FicNet) using multi-frequency Neighborhood (MFN) and double-cross modulation (DCM). Module MFN is adopted to capture the information in spatial domain and frequency domain. Then, the self-similarity and multi-frequency components are extracted to produce multi-frequency structural representation. DCM employs bi-crisscross component and double 3D cross-attention components to modulate the embedding process by considering global context information and subtle relationship between categories, respectively. The comprehensive experiments on three fine-grained benchmark datasets for two few-shot tasks verify that FicNet has excellent performance compared to the state-of-the-art methods. Especially, the experiments on two datasets, “Caltech-UCSD Birds” and “Stanford Cars”, can obtain classification accuracy 93.17% and 95.36%, respectively. They are even higher than that the general fine-grained image classification methods can achieve.

Index Terms—Few-shot learning, fine-grained image classification, feature modulation, multi-frequency component, weighted Neighborhood.

I. INTRODUCTION

Fine-grained image classification aims to accurately distinguish different sub-categories belonging to the same entry-level category, such as different kinds of birds, flowers, cars, etc. Particularly, with the development of deep learning [1], [2], some fine-grained classification methods based on neural network have attracted much attention in various application scenarios, such as automatic biodiversity monitoring [3] and intelligent detection [4]. Generally, fine-grained classification relies on a large number of labeled samples. However, there are only few training samples for some sub-categories in many fields, e.g. rare cases in medical research [5], unbalanced time series classification [6], new species in biological research [7]. Because of the obvious technical

merits, many few-shot learning (FSL) methods have been proposed to categorize the object images with few training samples in recent years [8], [9]. However, they can not capture the subtle features to deal with fine-grained classification task. Therefore, solving the few-shot fine-grained (FSFG) image classification task has attracted intensive attention. There still are some improvement space on FSFG learning because of the following three challenges: 1) the internal distances of sub-categories maybe very large; 2) the distances among sub-categories are small, i.e. there are only slight local difference; 3) many factors, such as viewing angle, background, and distance from camera, local variability and partial occlusion, may seriously affect the learning result. As shown in Fig. 1, posture and background bring large internal differences to the same category. In contrast, the bird’s beak or wings only have different colors for each column of the figure. The third challenge can be observed in the last query image in Fig. 1: there is only the head of a bird, and it is difficult to obtain good recognition by local block matching.

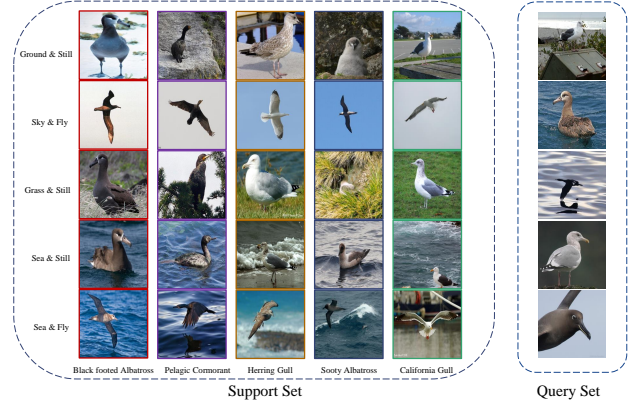


Fig. 1: Illustration of a “5-way 5-shot” FSFG task. Different columns represent different bird species: “Black footed Albatross”, “Pelagic Cormorant”, “Herring Gull”, “Sooty Albatross”, “California Gull”. Different rows represent different poses, “still” and “fly”, and different backgrounds, “ground”, “sky”, “grass”, and “sea”.

To address the first challenge, Wei et al. [10] augmented single coding feature with a self-bilinear encoding network and used a mapping network to learn decision boundaries for the input data. On this basis, Li et al. [11] proposed a covariance pooling to extract image representation for each class. To solve

This work was funded by the Natural Science Foundation of Liaoning Province (No. 2020-MS-080), the National Key Research and Development Program of China (No. 2017YFF0108800). (Corresponding author: Chengqing Li)

H. Zhu, Z. Gao, J. Wang and Y. Zhou are with the Department of Mathematics, College of Sciences, Northeastern University, Shenyang 110819, Liaoning, China (e-mail: zhuhegui@mail.neu.edu.cn).

C. Li is with MOE (Ministry of Education) Key Laboratory of Intelligent Computing and Information Processing, Xiangtan University, Xiangtan 411105, Hunan, China.

the second challenge, Zhu et al. [12] proposed a multi-attention method to get the discriminative parts of images. To obtain a more precise comparable feature representation, Huang et al. [13] proposed pairwise bilinear pooling network to extract comparative second-order descriptors for image pairs. Furthermore, they employed a new low-rank bilinear pool operation [14] to capture subtle differences between support set and query one. As it needs to consider the features distinguishing categories, which is different for different tasks, few methods were found to solve the third challenge. Moreover, the samples in the support set and query set may also respond to different parts of the target object.

In this paper, we propose a novel few-shot fine-grained image classification network (FicNet) using multi-frequency Neighborhood (MFN) and double-cross modulation (DCM). It not only captures discriminative information according to the task, but also extracts more portable and complete features of the target object. Furthermore, due to the influence of background and posture, the interference of spurious features and reliable relevant information are removed from the relationship structure of samples. The concrete technical contributions are summarized as follows:

- Proposing a novel and compact end-to-end network, which uses two branches of capture and modulation to solve FSFG classification.
- Designing module MFN to fuse spatial and frequency domain information, which can obtain multi-frequency structural representation.
- Designing module DCM to modulate feature from both context information and task-specific information.
- Experiments on two datasets, “Caltech-UCSD Birds” and “Stanford Cars”, are configured to demonstrate that the classification accuracy of FicNet exceeds that of the general fine-grained classification models.

The rest of the paper is organized as follows. First, the related work on fine-grained image classification and associate learning methods is briefly reviewed in Sec. II. Then, the adopted methodology to design FicNet is presented in Sec. III. Section IV presents detailed experimental settings and results to verify the effectiveness of FicNet. Furthermore, Sec. V provides extensive ablation studies on every basic part of FicNet. The last section concludes the paper.

II. THE RELATED WORK

To demonstrate the development background of FicNet, we briefly review the related work on few-shot learning, fine-grained image classification, few-shot fine-grained learning and frequency domain learning.

• Few shot learning:

FSL simulates human ability to acquire knowledge from a few samples through generalization and analogy. In recent years, many methods based on metric learning emerged. For example, Snell et al. [15] proposed a simple and efficient ProtoNet network for few-shot learning, which performed classification by calculating Euclidean distance from the prototype expression of each category; In [16], Zhang et al. proposed a second-order relational descriptors from feature

maps to capture the similarity between the query-support pairs. The most typical meta-learning method is the model-agnostic meta-learning algorithm (MAML) proposed by Finn et al. [17], which can learn a good set of initialization parameters. Furthermore, Wang et al. [18] devised a graph complemented latent representation (GCLR) network to learn a better representation. To alleviate over-fitting phenomenon in FSL from the estimation of data distribution, Yang et al. used calibrated distribution to provide more diverse generation [19].

• Fine-grained image classification:

For many years, fine-grained image classification has been a hot topic in the field of computer vision. Deep fine-grained classification methods can be broadly divided into two categories: regional features-based methods and global features-based methods. Zhang et al. first combined R-CNN into a fine-grained classifier with geometric prior, and used object detection to locate local regions [20]. For easy deployment, Zhang et al. [21] proposed a fine-grained image categorization system, which only classifies labels for training images. Different from simply locating different parts, the approach given in [22] attempted to mine complementary information from multiple granularity parts. The method designed in [23] can not only capture distinguishing parts, but also use knowledge in text description for interactive alignment. In contrast, the global features-based methods extract features from the whole image without explicit localization of the target. As a typical work, Feng [24] used kernel approximation to introduce high-order information, and then adopted statistical information to enhance modeling ability.

• Few-shot fine-grained learning:

Wei et al. [10] proposed the first FSFG model, which used self-bilinear encoder to capture subtle image features. Li et al. [11] further replaced the naive self-bilinear encoder with covariance pooling and designed covariance metric network, which measured the relationship between a query sample and each category by the distribution consistency. Different from these self-linear methods, Huang et al. [13] provided a novel pairwise-bilinear pooling method to compare subtle differences between fine-grained categories. Then they further employed a new low-rank bilinear pool operation [14], and designed a feature alignment layer to match the support features with the query features. Meanwhile, FOT [25] is a data enhancement method, which uses the posture transformation generator to generate additional samples of new sub-categories. Zhu et al. [12] proposed a multi-attention meta learning method that exploited the attention mechanism of base learner and task learner to capture the different parts of an image. Moreover, Ruan et al. [26] explored a spatial attentive comparison network (SACN), which consists of three separate modules for feature extraction, selective-comparison of similarity and classification.

• Frequency domain learning:

Ehrlich and Davis [27] creatively proposed a model-conversion algorithm to convert spatial-domain CNN model to frequency domain. Furthermore, Wang et al. [28] directly exploited the frequency modality as complementary information and capture the local contextual incoherence to

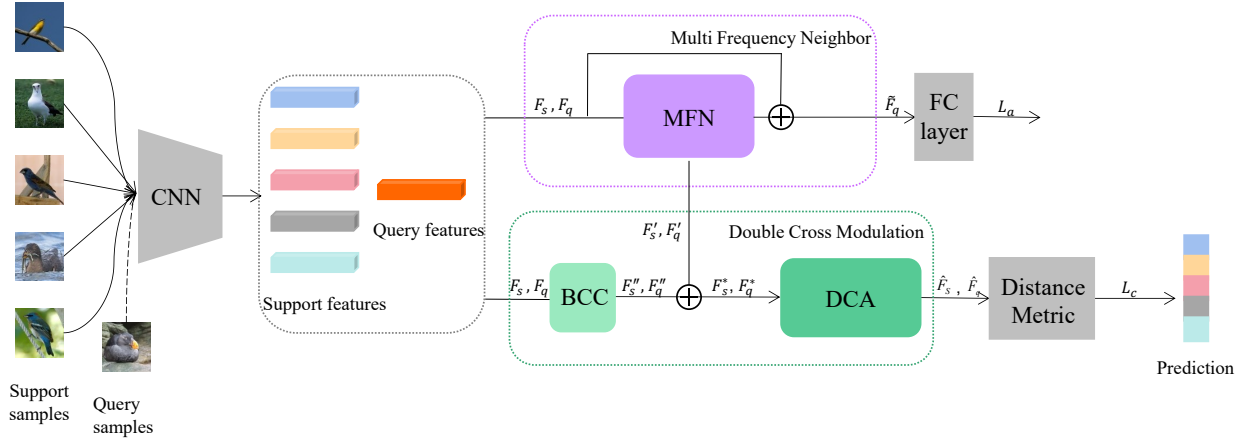


Fig. 2: The architecture of FicNet.

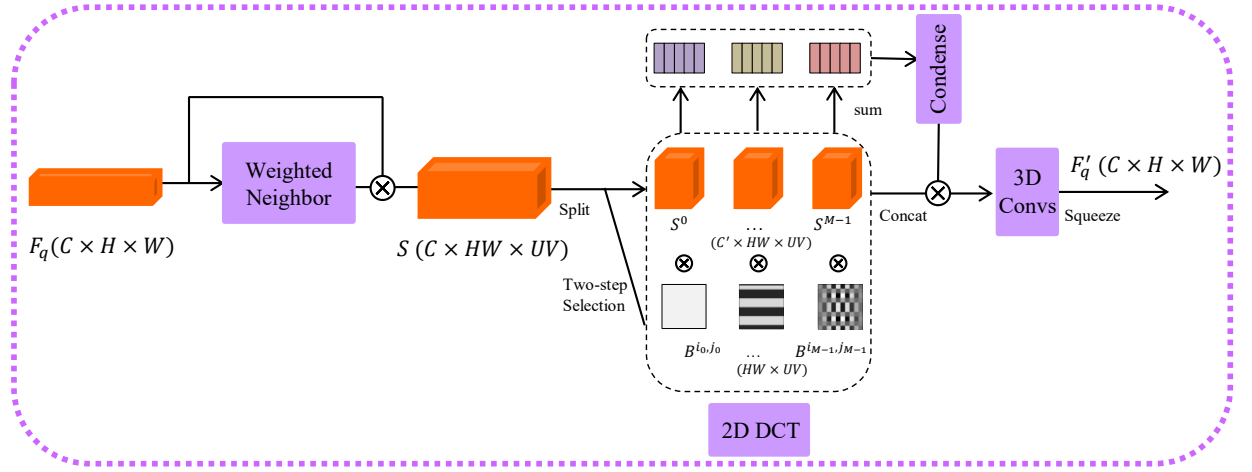


Fig. 3: The snapshot of module multi-frequency Neighborhood .

enhance boundary consistency. To avoid such complex model transition procedure, Xu et al. analyzed the spectral bias and provided a frequency selection method to identify the trivial frequency components [29]. Meanwhile, Qin et al. [30] started from a different view, and considered the channel representation problem as a compression process using frequency analysis. They proved that the conventional global average pooling is a special case of feature decomposition in the frequency domain.

Different from the previous image classification methods, FicNet try to solve FSFG problem from two branches of capture and modulation. First, it capture rich and compact structural patterns fusing space and frequency domain information to reduce the impact of intra-class appearance variation. Then it modulate the embedding process to contain more complete class-related details based on global context and task-specific information.

III. THE ADOPTED METHODOLOGY

A. Problem definition

A FSFG problem is usually formalized as a “ N -way K -shot” task, and the dataset is divided into two parts:

training set $D_{tr} = \{(I_i, y_i), y_i \in C^s\}_{i=1}^{N_{tr}}$ and testing set $D_{test} = \{(I_j, y_j), y_j \in C^t\}_{j=1}^{N_{test}}$, where I_i is the i -th fine-grained sample and y_i is its class label; the label sets satisfy $C^s \cap C^t = \emptyset$. We organized experiments in an episodic meta-training setting. Considering that both D_{tr} and D_{test} consist of many episodes, we randomly selected N different categories in each episode, and randomly choose K and P images in each category. They constitute support set $S = \{(I_s, y_s)\}_{s=1}^{NK}$ and query set $Q = \{(I_q, y_q)\}_{q=1}^{NP}$, respectively. Every episode is iteratively sampled from D_{tr} to train FicNet. Finally, we measured the average classification accuracy on query sets of many episodes from D_{test} .

B. Architecture overview

FicNet belongs to the metric-based methods, and the specific structure is shown in Fig. 2, which is composed of two main modules, MFN and DCM. Note that marker \oplus means element-wise sum, L_a denotes the auxiliary loss function, and L_c represents the classification loss. As for the input samples, we employed ConvNet-4 as the feature extractor to provide basic feature maps, which are converted into multi-frequency structural representations by analyzing the information in spa-

tial and frequency domain. Then, DCM combines bi-crisscross component (BCC) and double 3D cross-attention (DCA), where BCC efficiently generates global context to modulate multi-frequency structural representations, and DCA uses multiple 3D crossed convolution to perform modulation according to the current task. Finally, cosine distance is calculated to measure the similarity between the final representations.

C. Multi-frequency Neighborhood

The module MFN is employed to capture compact structural patterns by combining the information in spatial and frequency domain, which can reduce the change sensitivity of intra-class representations. It includes weighted Neighborhood and multi-frequency components. Figure 3 illustrates the overall structure of MFN, where \otimes represents the Hadamard product. The details of MFN are introduced as follows.

• Weighted Neighborhood :

Weighted Neighborhood encodes local invariant structure by associating each feature with neighborhood in spatial domain. Because the operations on the support set and the query set are the same, so only the operations of query image are illustrated here. Given a query image I_q , we employ ConvNet-4 to extract basic feature map $F_q \in R^{C \times H \times W}$. As for each position x in F_q , we extract its $UV - 1$ neighbors through the sliding window, where UV is the size of sliding block. Note that the nearer neighbor points obviously have a greater impact on x . So, one can obtain the different weighted neighbor representation

$$F_{q*}(x+e) = \frac{1}{\|e\| + 1} F_q(x+e),$$

where $x \in [0, H] \times [0, W]$, $e \in [-\frac{U+1}{2}, \frac{U-1}{2}] \times [-\frac{V+1}{2}, \frac{V-1}{2}]$. Then, one builds the local spatial representation $s \in R^{C \times H \times W \times U \times V}$ by aggregating information of each location x in F_q and its weighted neighbors F_{q*} into local spatial representation:

$$s(x, e) = \frac{F_q(x)}{\|F_q(x)\|} \otimes \frac{F_{q*}(x+e)}{\|F_{q*}(x+e)\|}.$$

• Multi-frequency components:

To further optimize the local spatial representation s , we convert it to frequency domain and represent it with frequency components. First, the local spatial representation s is reshaped into $S \in R^{C \times HW \times UV}$, and equally divided into M blocks along the channel dimension:

$$S = [S^0, S^1, \dots, S^{M-1}],$$

where channel dimension of each part S^m is $\frac{C}{m}$. Second, a two-dimensional DCT (2D-DCT) is employed on each part S^m :

$$\begin{aligned} Freq^m &= 2D - DCT^{i_m, j_m}(S^m) \\ &= \sum_{h=0}^{H-1} \sum_{w=0}^{W-1} S_{:,h,w}^m B_{h,w}^{i_m, j_m}, \end{aligned}$$

where $m \in \{0, 1, \dots, M-1\}$, and (i_m, j_m) is the index of the frequency component corresponding to $Freq^m$. In particular, the basis function $B_{h,w}^{i_m, j_m}$ is a pre-calculated

constant, so this process does not introduce parameters. Moreover, the selection of index (i_m, j_m) is also a key issue, and its detailed procedures are given as follows:

- **Step 1** For each possible alternative frequency component corresponding to index (m_i, m_j) , evaluate the performance of the model using each component separately, where $m_i \in \{0, 1, \dots, H-1\}$, $m_j \in \{0, 1, \dots, W-1\}$. If the frequency component can bring higher classification accuracy, it is considered to be more important.
- **Step 2** Produce the top- M frequency components according to the importance demonstrated in **Step 1**: $\{(i_1, j_1), \dots, (i_{M-1}, j_{M-1})\}$.

Then we integrate the scattered frequency information to get multi-frequency feature

$$D = \text{Sigmoid}(\text{fc}([Freq^0, Freq^1, \dots, Freq^{M-1}])), \quad (1)$$

where fc is the fully connected layer, and activation function $\text{Sigmoid}(x) = \frac{e^x}{e^x + 1}$. Finally, we obtain the multi-frequency structural representation

$$F'_q = \text{Conv}_{3d}(D \otimes S),$$

where Conv_{3d} represents the 3D convolution for dimension reduction.

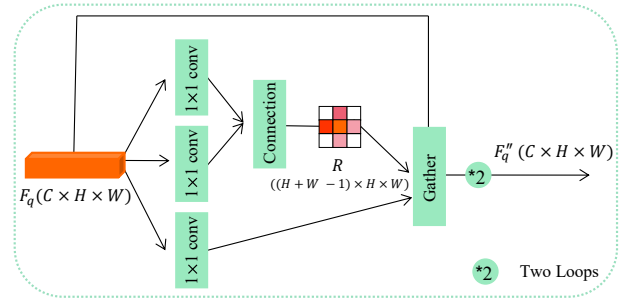


Fig. 4: The structure of bi-crisscross component.

D. Double-cross Modulation

To modulate representation F'_q more complete and adapt to the current task, DCM is adopted to modulate feature from both context information and task-specific information. First, we use BCC to generate global context information, which is a supplement to the multi-frequency structural representation F'_q . Then, DCA is used to adjust target region according to the current task:

• Bi-crisscross component:

Figure 4 depicts the detailed contents of BCC. As for the given basic feature map $F_q \in R^{C \times H \times W}$ corresponding to query image I_q , do the following bi-crisscross operations on F_q :

- **Step 1** F_q is fed into two 1×1 convolution layers to reduce channel dimension into C'' and a plain 1×1 convolution layer to generate three feature maps Q , K , and V , where $Q, K \in R^{C'' \times H \times W}$ and $V \in R^{C \times H \times W}$. Denote feature vectors of K and V in the same position as sets $\Omega_p \in R^{(H+W-1) \times C''}$ and $\Phi_p \in R^{(H+W-1) \times C}$, respectively.

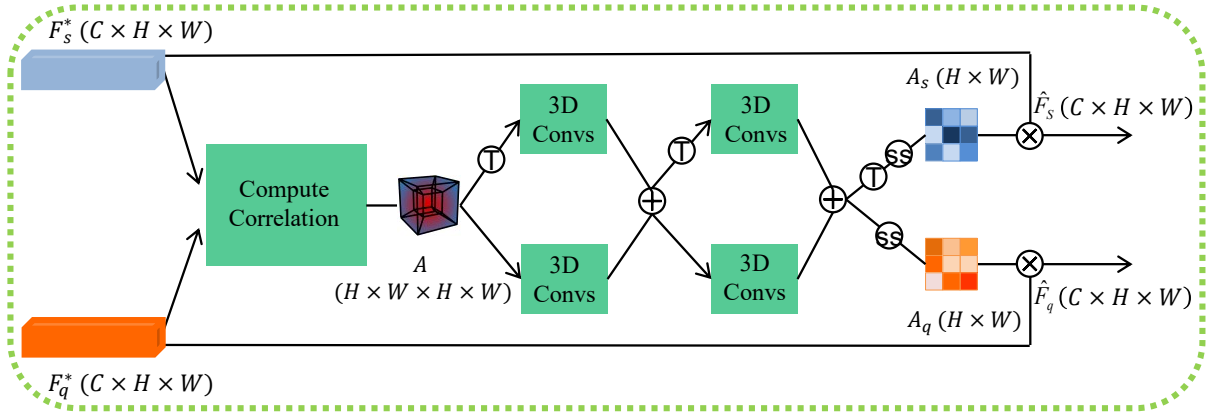


Fig. 5: The structure of DCA, where \otimes represents sum after Softmax, \top represents transpose.

–**Step 2** Use connection operation to extract information in the horizontal and vertical directions by

$$R(i, p) = \text{Softmax}(Q_p \Omega_{i,p}^\top), \quad (2)$$

where Softmax is the activation function, Q_p is a feature vector of Q at position p , $\Omega_{i,p} \in R^{C''}$ is the i -th element of Ω_p , $R(i, p)$ is a vector on $R \in R^{(H+W-1) \times H \times W}$ that reveals the degree of correlation between feature Q_p and $\Omega_{i,p}$, and $i \in \{1, 2, \dots, H+W-1\}$.

–**Step 3** Do the gather operation to aggregate the context information of each pixel in the cross path by

$$\text{gather}(R(i, p), \Phi_p, F_q(p)) = \sum_{i=1}^{H+W-1} R(i, p) \Phi_{i,p} + F_q(p),$$

where $\Phi_{i,p} \in R^{C''}$ is the i -th element of Φ_p , $F_q(p)$ is the feature vector of F_q at position p .

–**Step 4** Repeat the crisscross operations in Steps 1, 2, 3 twice and obtain F_q'' , which act as complement to modulate F_q' , and obtain the multi-frequency complete feature

$$F_q^* = F_q'' + F_q'.$$

Note that the operations on the support samples are the same as that on the query samples. The prototype F_s^* of support samples S can be obtained in a class-average manner.

• **Double 3D cross-attention:**

To make modulation adapt to the current task, DCA takes a pair of support prototype F_s^* and query F_q^* to produce the corresponding cross-attention maps A_s and A_q , respectively. Figure 5 shows the pipeline of DCA. First, calculate the correlation map $A \in R^{H \times W \times H \times W}$ with cosine distance, where the correlation degree of position x_s in F_s^* and x_q in F_q^* can be obtained by

$$A(x_s, x_q) = \left(\frac{F_s^*(x_s)}{\|F_s^*(x_s)\|_2} \right)^\top \left(\frac{F_q^*(x_q)}{\|F_q^*(x_q)\|_2} \right),$$

where $x_s, x_q \in [0, H] \times [0, W]$. Then use 3D double-cross convolutions to refine the 4-dimensional tensor A with the following steps:

–**Step 1** Reshape tensor A from $R^{H \times W \times H \times W}$ into $R^{1 \times H \times W \times HW}$, and regard the last dimension of A as the time dimension and feed it into 3D convolution.

–**Step 2** Perform the same operations on A^\top ; reshape time dimensions of two results from HW into $H \times W$ and add them to produce A^1 .

–**Step 3** Crossly feed A^1 into two $3 \times 3 \times 3$ convolutions, and integrate the results as cross-attention map $A' \in R^{H \times W \times H \times W}$.

–**Step 4** Transform A' into cross-attention map $A_q \in R^{H \times W}$ by

$$A_q(x_q) = \frac{\exp\left(\frac{\sum_{x_s} A'(x_s, x_q)/T}{|x_s|}\right)}{\sum_{x'_q} \exp\left(\frac{\sum_{x_s} A'(x_s, x'_q)/T}{|x_s|}\right)}, \quad (3)$$

where $|x_s| = HW$, $T \in (0, 1]$ is the temperature coefficient, $A_q(x_q)$ represents the average matching probability between two elements in the query sample and support prototype at position x_q . Similarly, cross attention map $A_s \in R^{H \times W}$ of support prototype can be calculated by Eq. (3).

Finally, A_q and A_s are used to modulate F_s^* and F_q^* , and get the final representations

$$\begin{cases} \hat{F}_q = A_q F_q^*, \\ \hat{F}_s = A_s F_s^*, \end{cases} \quad (4)$$

which are used to fuse reliable semantic-related information between them and highlight the relevant regions.

E. Learning flow

FicNet finally uses metric classification for the final representation. Note that it is end-to-end trainable from scratch. The loss function and training steps of FicNet are introduced as follows in detail.

• **Metric classification:**

As for a “ N -way K -shot” task, N support categories yield N different attention maps. So, one can obtain N different support representations $\{\hat{F}_s^{(i)}\}_{i=1}^N$ and the corresponding query representations $\{\hat{F}_q^{(i)}\}_{i=1}^N$. Then, compute the similarity between query representations $\{\hat{F}_q^{(i)}\}_{i=1}^N$ and support

prototypes $\{\hat{F}_s^{(i)}\}_{i=1}^N$ with cosine distance, and then classify query representation into the nearest support category.

• **Loss function:**

FicNet adopts a single-stage training method, and combines two classification losses for end-to-end learning. As for module MFN, we classify the query feature $\tilde{F}_q = F_q + F'_q$ by adding an additional full connection layer (the layer FC is only used in the training stage), and calculate the cross entropy loss

$$L_a = -\log \frac{\exp(w_c^\top \tilde{F}_q + b_c)}{\sum_{c=1}^{N_{tr}} \exp(w_c^\top \tilde{F}_q + b_c)}$$

as the auxiliary loss to guide the learning of feature extractor CNN and the module MFN, where N_{tr} is the total number of categories in the train set, w_c^\top and b_c are the weight and bias in the layer FC, respectively. On the other hand, as for the final representations \hat{F}_s, \hat{F}_q output by DCM, we build a metric classification loss L_c . Considering that FSFG problem may contain difficult negative samples, we use contrast loss

$$L_c = -\log \frac{\exp(\text{dis}(\hat{F}_s^{(i)}, \hat{F}_q^{(i)})/t)}{\sum_{i'=1}^N \exp(\text{dis}(\hat{F}_s^{(i')}, \hat{F}_q^{(i')})/t)}$$

as the classification loss, where $\text{dis}(\cdot, \cdot)$ is cosine similarity, the temperature coefficient t is set as 0.2. The above loss function guides the model to learn the feature space, where the query samples are measured and classified correctly. Finally, the total loss function is

$$L = L_c + \mu L_a, \quad (5)$$

where μ is hyper-parameter that balances the loss term.

• **Training procedure**

The pseudocodes for implementing the meta-training process are given in given in Algorithm 1.

IV. PERFORMANCE EVALUATION

Four benchmark datasets and the experimental details are first introduced to support the following performance evaluation of FicNet over some state-of-the-art methods ¹.

A. Datasets

FicNet is evaluated on three fine-grained benchmark datasets: CUB-200 (200 kinds of birds, 11,788 images) [31], Stanford Dogs (120 kinds of dogs, 20,580 images) [32], Stanford Cars (196 kinds of cars, 16,185 images) [33]. In addition, we also tested the generalization ability of FicNet on a general image classification dataset, mini-ImageNet [8]. It is a subset of ImageNet [34] and consists of 60,000 images distributed over 100 different categories. For fair performance comparison, we adopt the data split method used in [26], [35]. The original images are divided into two disjoint subsets: the auxiliary training set and testing set. For each category in the auxiliary training set, we divide the data into training

Algorithm 1: Meta-training phase.

Input : $D_{tr} = \{(I_i, y_i), y_i \in C^s\}_{i=1}^{N_{tr}}$; learning rate α ; hyper-parameter μ

Output: Trained model $\varphi \subseteq \{\varphi_{cnn}, \varphi_{mfn}, \varphi_{dcm}\}$

- 1 Randomly initialize model parameters $\varphi_{cnn}, \varphi_{mfn}, \varphi_{dcm}$; Initialize loss $L = 0$;
- 2 **while not done do**
- 3 Sample batch of episodes $T \sim D_{tr}$, a task T_i includes a support set $S = \{(I_s, y_s)\}_{s=1}^{N_{tr}}$ and a query set $Q = \{(I_q, y_q)\}_{q=1}^{N_{P}}$;
- 4 **for all** T **do**
- 5 **for all samples in** T_i **do**
- 6 $F_s, F_q \leftarrow \varphi_{cnn}(I_s, I_q)$;
- 7 $F'_s, F'_q, \tilde{F}_s, \tilde{F}_q \leftarrow \varphi_{mfn}(F_s, F_q)$;
- 8 $L_a(\varphi) \leftarrow \frac{1}{N_P} \sum_{(\tilde{F}_q, y) \in Q} L_a(\tilde{F}_q, y)$;
- 9 $\hat{F}_s, \hat{F}_q \leftarrow \varphi_{dcm}(F_s, F'_s, F_q, F'_q)$;
- 10 $L_c(\varphi) \leftarrow \frac{1}{N_P} \sum_{(\hat{F}_q, y) \in Q} L_c(\hat{F}_q, y)$;
- 11 $L_{T_i}(\varphi) \leftarrow L_c(\varphi) + L_a(\varphi)$;
- 12 **end**
- 13 **end**
- 14 $\varphi \leftarrow \varphi - \alpha \frac{1}{|T|} \sum_{T_i} L_{(T_i)}(\varphi)$;
- 15 **end**

dataset and validation dataset. The former is used for training parameters and the latter is employed to monitor the learning process. The details of the mentioned four datasets are shown in Table I.

TABLE I: The category split of four benchmark datasets, where N_{total} is the original total number of categories in the datasets; N_{tr} , N_{val} and N_{test} are the numbers of categories in the train set, validation set, and test set, respectively.

Dataset	N_{total}	N_{tr}	N_{val}	N_{test}
CUB-200	200	120	30	50
Stanford Dogs	120	70	20	30
Stanford Cars	196	130	17	49
mini-ImageNet	100	64	16	20

B. Experimental configuration

For fair and extensive comparison, we employ ConvNet-4, ResNet-12 as different backbones followed with the recent FSFG classification works [12], [13], [26], [35]. All the samples used for training and testing are resized to 84×84 . We set $U = V = 5$ for module MFN. As for module DCM, considering memory and time, the size of 3D convolutions is set as $3 \times 3 \times 3$, T of DCA is set as 1 for “Stanford Dogs” and 2 for others; parameter μ in Eq. (5) is set as 0.7; SGD is used to optimize the parameters and the learning rate α is initially set as 0.1. We use the episodic training paradigm to train FicNet. For the “ N -way K -shot” task, we randomly select N categories, and randomly get K samples from each category as the support set, and then randomly choose 15 samples as the query set for evaluation. Finally, we report

¹The source codes of this paper are available at <https://github.com/ChengqingLi/FicNet>

top-1 average classification accuracy with 95% confidence intervals of randomly sampled 1,200 test episodes. The model is implemented by PyTorch on Tesla K80.

C. Comparison with the state-of-the-art methods

To evaluate the effectiveness of FicNet on fine-grained datasets, we compared it with some state-of-the-art methods, including several specific FSFG methods and four typical FSL methods. Table II lists the comparison results on three fine-grained datasets, CUB-200, Stanford Dogs, Stanford Cars, with standard “5-way 1-shot” and “5-way 5-shot” tasks, where ConvNet-4 and ResNet-12 are adopted as backbone network. Among the precious reference counterparts, the best results and the second best ones are marked with dashed underline and wavy underline, respectively. Specially, the numbers beside symbol \uparrow indicates improvement percentage of FicNet with respect to the second best result.

From Table II, one can see that when ConvNet-4 is used as the feature extractor, FicNet can achieve improvement 3.77%, 0.44% and 9.08% over the second best method on the three datasets for the “5-way 1-shot” task, respectively. As for the “5-way 5-shot” task, FicNet achieves accuracy improvement 5.17%, 6.03% and 0.31% over the second best method on the three datasets, respectively. When Resnet-12 is used as the feature extractor, FicNet also significantly outperforms the other comparable methods: it can obtain an average accuracy of 80.97%, 72.41% and 86.81% on the three datasets for the “5-way 1-shot” task, respectively. As for the above task, the corresponding accuracy ratios are 93.17%, 85.11%, and 95.36% for the “5-way 5-shot” task, respectively. Due to the limitation of presentation space, only some typical results are given in Table II. Therefore, the effectiveness of FicNet is unrelated with selected backbone, verifying its robustness and compatibility.

D. Generalization ability on the general FSL tasks

To illustrate the generalization ability of FicNet, we performed experiments on mini-ImageNet. Most recent classification methods [44]–[46] use deeper convolutional neural networks as feature extraction backbones, such as ResNet family. Therefore, we selected ResNet-12 as backbone to perform the comparative experiment with the “5-way 1-shot” and “5-way 5-shot” tasks.

As can be seen from Table III, even compared with those methods whose backbone network is ResNet-18, ResNet-34 or WRN-28-10, FicNet still demonstrates better performance, where “+” denotes larger backbones than ResNet-12. The number beside symbol \uparrow indicates change between FicNet over baseline (ProtoNet*). As for “1-shot” and “5-shot” tasks, the classification accuracy of FicNet can reach 67.82% and 82.71%, respectively. The results are superior to all the other state-of-the-art methods, verifying that FicNet has high stability and strong generalization.

E. Visualization results

To further verify the performance of FicNet in a visual way, we performed the t-distributed stochastic neighbor embedding

(t-SNE) visualization. We randomly selected three “5-way 5-shot” tasks on dataset CUB, and each task included 25 support samples and 175 query samples. The t-SNE visualizes feature distributions of basic extraction feature, module MFN and modul DCM are shown in Fig. 6, where each row represents a “5-way 5-shot” task, and each column represents the corresponding feature distribution.

From Fig. 6(a)-(b), one can see that the samples belonging to the same category are gradually clustered together and the intra-class distance decreases significantly, which indicates that MFN can learn discriminative class-invariant features. From Fig. 6(b)-(c), one can intuitively observe that the inter-class distance becomes larger and the classification boundary is clearer. In particular, in Fig. 6(b), there are some samples that distribute at the edge or far from the true category center, which are prone to be misclassified. After we used DCM to do modulation based on global information and task-specific information, the misclassified samples are pulled back to the correct position, which illustrates that DCM can obtain complete and adaptive features that are conducive for good sample matching.

V. ABLATION STUDY

To illustrate the effects of different modules of FicNet, we provide extensive ablation studies using ResNet-12 as backbone.

A. The effect analysis of different module

To evaluate the effect of module MFN and module DCM, we conducted experiments with “5-way 1-shot” and “5-way 5-shot” tasks on dataset CUB, where ProtoNet* is used as the baseline. Table IV shows the specific experimental results including accuracy and the number of additional parameters. Note that if the module is employed to FicNet, it is represented with “+” or “-” otherwise.

As can be observed from Table IV, compared with the baseline, MFN achieves improvements 5.78% and 5.84% on “1-shot” and “5-shot” tasks, respectively. In contrast, DCM can achieve improvements 5.54% and 6.23% on the two tasks, respectively. They also verifies the effectiveness of MFN and DCM. Moreover, combining two modules MFN and DCM can achieve classification accuracy 80.97% and 93.17% for the two tasks, respectively. These results verify that the two modules are orthogonal and complementary, and MFN and DCA are both effective for solving the FSFG problem.

B. The performance analysis of MFN

To further illustrate the effectiveness and generalization of MFN, we provided experiments on the frequency component and its number in MFN, and analyzed the performance with other methods.

• Influence of individual frequency components:

To study the impact of different frequency components on the performance of MFN, we use only one frequency component of FicNet at a time to evaluate the separate classification accuracy. We divided the two-dimensional DCT

TABLE II: Classification accuracy (%) comparison of FicNet with typical FSFG image classification methods on three datasets.

Method	Backbone	CUB-200		Stanford Dogs		Stanford Cars	
		5-way 1-shot	5-way 5-shot	5-way 1-shot	5-way 5-shot	5-way 1-shot	5-way 5-shot
Matching Net [8]	ConvNet-4	45.30±1.03	59.50±1.01	35.80±0.99	47.50±1.03	34.80±0.98	44.70±1.03
ProtoNet [15]		37.36±1.00	45.28±1.03	37.59±1.00	48.19±1.03	40.90±1.01	52.93±1.03
MAML [17]		54.92±0.95	73.18±0.77	44.64±0.89	60.20±0.80	46.71±0.89	60.73±0.85
RelationNet [36]		59.58±0.94	77.62±0.67	43.05±0.86	63.42±0.76	45.48±0.88	60.26±0.85
PCM [10]		42.10±1.96	62.48±1.21	28.78±2.33	46.92±2.00	29.63±2.38	52.28±1.46
GNN [37]		51.83±0.98	63.69±0.94	46.98±0.98	62.27±0.95	55.85±0.97	71.25±0.89
CovaMNet [11]		52.42±0.76	63.76±0.64	49.10±0.76	63.04±0.65	56.65±0.86	71.33±0.62
DN4 [38]		46.84±0.81	74.92±0.64	45.41±0.76	63.51±0.62	59.84±0.80	88.65±0.44
PABN+cpt [13]		63.36±0.80	74.71±0.60	45.65±0.71	61.24±0.62	54.44±0.71	67.36±0.61
LRPABN+cpt [14]		63.63±0.77	76.06±0.58	45.72±0.75	60.94±0.66	60.28±0.76	73.29±0.58
ATL-Net [39]		60.91±0.91	77.05±0.67	54.49±0.92	73.20±0.69	67.95±0.84	89.16±0.48
BSNet (R&C) [35]		65.89±1.00	80.99±0.63	51.06±0.94	68.60±0.73	54.12±0.96	73.47±0.75
FOT [25]		67.46±0.68	83.19±0.43	49.32±0.74	58.83±0.85	54.55±0.73	73.69±0.65
TOAN [40]		65.34 ±0.75	80.43±0.60	49.30±0.77	67.17±0.49	65.90±0.72	84.24±0.48
SACN [26]		71.50±1.62	79.77±0.96	64.30±1.74	71.65±1.00	68.23±1.69	78.70±1.00
DLG [41]		64.77±0.90	83.31±0.55	47.77±0.86	67.07±0.72	62.56±0.82	88.98±0.47
NDPNet [42]	\	64.74±0.90	80.52±0.63	56.21±0.86	74.82±0.84	71.48±0.89	91.92±0.91
BSNet (R&C) [35]		69.73±0.97	82.85±0.61	58.83±0.85	76.60±0.69	66.97±0.99	84.09±0.66
MML (KL) [43]		—	—	59.05±0.23	75.59±0.21	72.43±0.25	91.05±0.23
FOT [25]		72.56 ±0.65	87.22±0.35	—	—	—	—
FicNet	ConvNet-4	75.27±0.61	88.48±0.37	64.74±0.69	79.23±0.46	77.31±0.58	89.47±0.32
Trend		↑ 3.77	↑ 5.17	↑0.44	↑ 6.03	↑ 9.08	↑ 0.31
FicNet	ResNet-12	80.97±0.57	93.17±0.32	72.41±0.64	85.11±0.37	86.81±0.47	95.36±0.22
Trend		↑ 8.41	↑ 5.95	↑ 8.11	↑ 8.51	↑ 14.38	↑ 3.44

\ NDPNet uses a novel feature re-abstraction network as the extractor.

- Neither experiment results on the specified settings nor open source codes are available for the corresponding method, so accurate comparison results are unavailable.

TABLE III: Classification accuracy (%) comparison on mini-ImageNet dataset.

Method	Backbone	mini-ImageNet	
		5-way 1-shot	5-way 5-shot
MatchNet [8]	ResNet-12	63.08±0.80	75.99±0.60
cosine classifier [44]		55.43±0.81	77.18±0.61
ProtoNet* [15]		62.39±0.21	80.53±0.14
TADAM [44]		58.50±0.30	76.70±0.30
CAN [45]		63.85±0.48	79.44±0.34
RFS-simple [47]		62.02±0.63	79.64±0.44
NegMargin [48]		63.85±0.81	81.57±0.56
DeepEMD [46]		65.91±0.82	82.41±0.56
MATANet [9]		60.13±0.81	75.42±0.72
FEAT [31]		66.78±0.20	82.05±0.14
InfoPatch [49]		67.67±0.45	82.44±0.31
RENet [50]		67.60±0.44	82.58±0.30
GCLR [18]		62.53±0.64	80.34±0.47
MixtFSL [51]		63.98±0.79	82.04±0.49
MLSo+PN [16]		66.08±1.80	82.32±0.66
PPA [52]	WRN-28-10 ⁺	59.60±0.41	73.74±0.19
PSST [53]		64.16±0.44	80.64±0.32
wDAE-GNN [54]	ResNet-34 ⁺	61.07±0.15	76.75±0.11
S2M2 [55]		63.74±0.18	79.45±0.12
DC [56]	ResNet-18	62.53±0.19	79.77±0.19
FicNet	ResNet-12	67.82±0.56	82.71±0.40
Trend		↑ 5.43	↑ 2.18

TABLE IV: Effects of MFN and DCM.

MFN	DCM	1-shot	5-shot	#added params
-	-	73.13	85.03	0K
+	-	78.91	90.87	254.11K
-	+	78.67	91.26	551.06K
+	+	80.97 (↑ 7.84)	93.17 (↑ 8.14)	805.17K

frequency space into 5×5 blocks, and constructed 25 experiments on mini-ImageNet with “5-way 1-shot” task. The experimental results are shown in Fig. 7 in a form of 5×5 matrix. First, the lower frequency components generally have better performance. Second, their accuracy are different no matter the frequency components are close or far, which show that different frequency components contains different information, and dispels the doubt that the use of multiple frequency components brings information redundancy. Finally, among all frequency components, the difference in classification accuracy is within 2%. Therefore, even if multiple frequency components are not selected in a targeted manner, it can bring a certain degree of performance improvement, which strongly illustrates that it is an effective innovation to combine information in spatial domain and frequency domain to encode the features.

• Influence of the number of frequency components:

To illustrate the influence of the number of frequency components M on model accuracy, we chose $M = 1, 2, 4, 8, 12, 16, 25$ to do experiments on dataset CUB. The results are shown in Fig. 8, demonstrating that the classification accuracy increases obviously with increasing of the number of multiple frequency components from 2 to 12 for the “5-way 1-shot” and “5-way 5-shot” tasks. This is attributed to that different frequency components contain different information, and more information can be extracted from the frequency domain. Moreover, two curves reach peak values 80.97% and 93.17% at $M = 12$, respectively. This also means that 12 frequency components are sufficient to capture useful features. Therefore, M is set as 12 in FicNet.

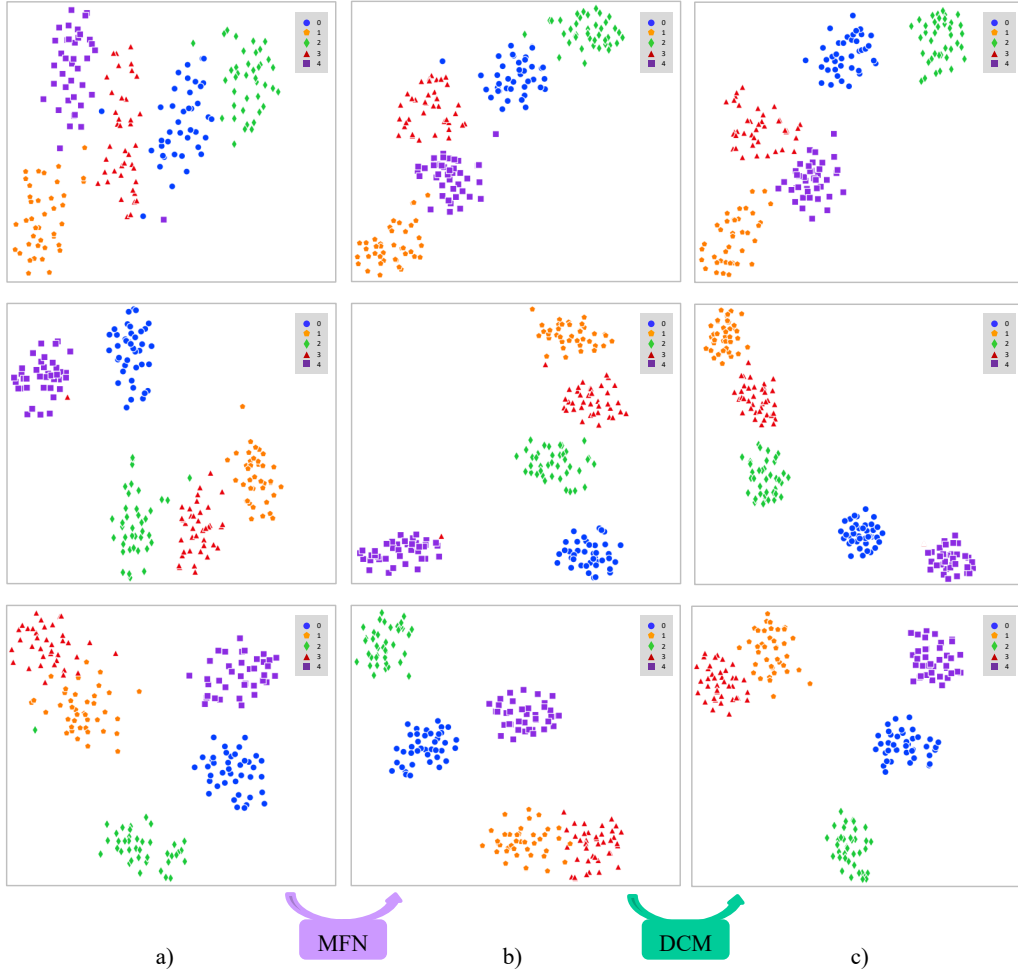


Fig. 6: t-SNE visualization results of FicNet: a) distribution of basic features; b) distribution of multi-frequency structural features; c) distribution of final features.

• The combination of MFN with the other methods

To show MFN can provide invariant structural representations, we explored its generalization and applicability by combining it with the other models. Here, we combine ProtoNet* in [15] and CAN in [45] with MFN to illustrate the performance. Table V lists the classification accuracy of datasets CUB and mini-ImageNet with “5-way 1-shot” task. As can be seen from Table V, MFN improves the accuracy of ProtoNet* by 5.78% on dataset CUB and 4.43% on dataset mini-ImageNet. It also obtains improvement 1.96% and 3.08% over the results obtained with running CAN on the two datasets, respectively. All these results convince us that MFN can boost the other methods significantly.

TABLE V: Results of combining MFN with other methods.

method	CUB-200	mini-ImageNet
ProtoNet* [15]	73.13	62.39
ProtoNet*+MFN	78.91	66.82
CAN [45]	77.22	63.85
CAN+MFN	79.18	66.93

• The comparison performance of MFN and the other similarity-based modules.

To show the effectiveness of MFN, we compared it with the other similarity-based modules by adding them to the baseline model ProtoNet*. The module SCE in [57] calculates the cosine similarity between the reference position and its adjacent ones, and connects their similarity in a fixed order of channel dimension. On the contrary, MFN does not limit the observation of different neighborhood relationships. SCR in [50] uses self-similarity to learn the relationship pattern of “how each feature is related to its neighbors”. However, it does not take into account that different neighbors have different importance. MFN uses weighted neighbors and integrates frequency domain information to capture more compact structural patterns. From Table VI, one can see that MFN outperforms all the other similarity-based modules, verifying the effectiveness of MFN.

C. The analysis of DCM module

To deeply illustrate the performance of DCM, we studied how to select the number of crisscross operations of BCC and analyze the performance of BCC and DCA for the modulation.

• Influence of the number of crisscross operation

To show the effect of using different number of crisscross operation in BCC, Fig. 9 depicts the variation curve of

65.73	65.61	65.36	65.29	64.45
64.72	65.42	64.82	64.50	64.33
65.69	64.47	64.81	64.99	64.14
65.09	64.60	64.61	64.10	63.80
64.19	64.09	63.84	63.81	63.73

Fig. 7: Classification accuracy(%) on mini-ImageNet using different frequency component.

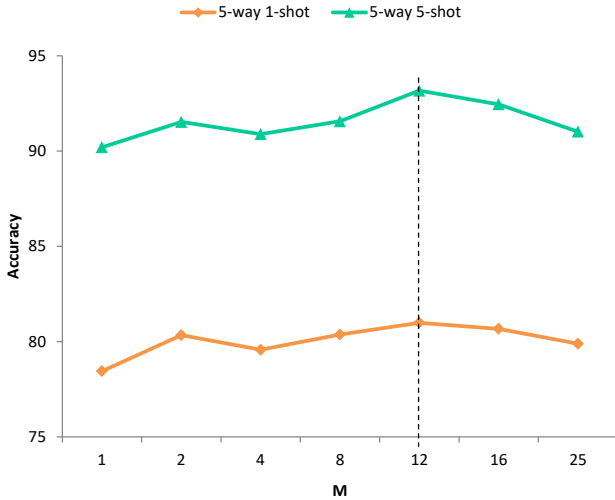


Fig. 8: Experimental results of FicNet using different number of frequency components.

TABLE VI: Comparison with the other similarity-based modules.

method	CUB-200	mini-ImageNet
Baseline	73.13	62.39
Baseline+SCE [57]	77.85	63.19
Baseline+SCR [50]	78.09	66.18
Baseline+MFN	78.91	66.82

classification accuracy, memory and time with the number L . From Fig. 9, after adding BCC component into FicNet, the performances for “1-shot” and “5-shot” tasks are improved by 1.11% and 1.16%, respectively. This can effectively demonstrates the importance of supplementing context information. Then, if increase number L from 1 to 2, the model can improve the performance under the above two tasks by

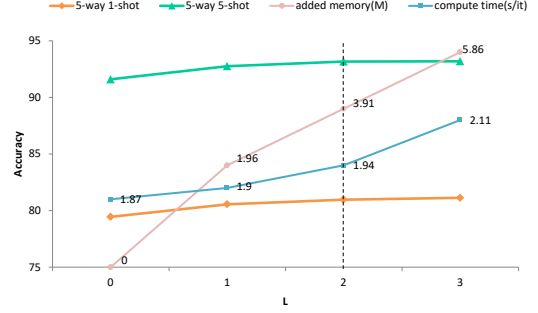


Fig. 9: Experimental results of FicNet using different number of crisscross operations.

0.41% and 1.16%, respectively. Furthermore, in Fig 9, we also observe the memory occupancy and computation time continues to increase with respect to L . Therefore, to balance the performance and computational resources, $L = 2$ is optimal for FicNet.

• Effect analysis of BCC and DCA of DCM

To study the effect of BCC and DCA of DCM, we employed ablation experiments on dataset CUB for “1-shot” and “5-shot” tasks. Note that if the module is employed to FicNet, it is represented with “+”, and “-” otherwise. The results are illustrated in Table VII, which show that BCC achieves improvements 0.27% and 0.15% over the baseline for “1-shot” and “5-shot” tasks. In contrast, DCA obtains improvements 1.02% and 0.45% over the two tasks, respectively. Moreover, combining BCC and DCA can achieve classification accuracy improvement 2.06% and 2.3% over the baseline for the two tasks, respectively. All these verified that the combination of BCC and DCA can further improve the classification accuracy and bring benefits to the model, which also shows that it is necessary to integrate the global context information into the embedding process.

TABLE VII: Effects of BCC and DCA component of the DCM module.

DCM		1-shot	5-shot
BCC	DCA		
-	-	78.91	90.87
+	-	79.18	91.02
-	+	79.93	91.32
+	+	80.97	93.17

• The comparable performance of DCA and CAN

To further analyze the performance of DCA, we constructed experiments with DCA and CAN. Similar to DCA, CAN also focuses on task-specific information, and directly averages 4D cross-correlation into 2D tensor. Compared with CAN, DCA uses 3D double-cross convolutions to refine the 4D cross-correlation tensor while maintaining the details of geometric space. The comparison results are shown in Table VIII. As shown in the first two rows of Table VIII, when replacing CAN with DCA component, the classification accuracy is improved by 0.81% and 1.2% on two

datasets, CUB and mini-ImageNet, respectively. The results show that DCA can avoid the collapse of key details caused by CAN, and obtain more reliable task level attention. In addition, the last two rows of Table VIII demonstrate that the classification accuracy can be improved after adding BCC components for either module.

TABLE VIII: Comparison results of DCA and CAN.

method	CUB-200	mini-ImageNet
CAN	77.22	63.85
DCA	77.93	65.03
MFN+CAN	79.18	66.93
MFN+DCA	79.93	67.21
MFN+BCC+CAN	80.02	67.25
MFN+BCC+DCA	80.97	67.82

VI. CONCLUSION

In this paper, we designed a high-accuracy few-shot fine-grained image classification method by capturing the spatial and frequency information of the classified images with two modules MFN and DCM. The former obtained multi-frequency structural representation, and could bring a certain degree of performance improvement. The latter modulated feature from both global context and task-specific information. The proposed method did not require bounding box or part annotation in new representation for metric classification. Extensive experiments demonstrated that it outperforms the previous state-of-the-art counterparts on some fine-grained datasets. However, its performance may be less significant when dealing with richer datasets. Extending its generalization and effectiveness to efficiently deal with more complex scenes and computer vision tasks, such as salient object detection, deserves further exploring.

REFERENCES

- [1] S. Zhou, Y. He, Y. Liu, C. Li, and J. Zhang, "Multi-channel deep networks for block-based image compressive sensing," *IEEE Transactions on Multimedia*, vol. 23, pp. 2627–2640, 2021.
- [2] S. Zhou, X. Deng, C. Li, Y. Liu, and H. Jiang, "Recognition-oriented image compressive sensing with deep learning," *IEEE Transactions on Multimedia*, 2022.
- [3] G. Van Horn, E. Cole, S. Beery, K. Wilber, S. Belongie, and O. Mac Aodha, "Benchmarking representation learning for natural world image collections," in *Proceedings of The IEEE/CVF Conference on Computer Vision and Pattern Recognition*, 2021, pp. 12 879–12 888.
- [4] L. Guan, L. Jia, Z. Xie, and C. Yin, "A lightweight framework for obstacle detection in the railway image based on fast region proposal and improved yolo-tiny network," *IEEE Transactions on Instrumentation and Measurement*, vol. 71, no. 5009116, 2022.
- [5] R. Feng, X. Zheng, T. Gao, J. Chen, W. Wang, D. Z. Chen, and J. Wu, "Interactive few-shot learning: limited supervision, better medical image segmentation," *IEEE Transactions on Medical Imaging*, vol. 40, no. 10, pp. 2575–2588, 2021.
- [6] H. Zhu, R. Xiao, J. Zhang, J. Liu, C. Li, and L. Yang, "A driving behavior risk classification framework via the unbalanced time series samples," *IEEE Transactions on Instrumentation and Measurement*, vol. 71, p. 2503312, 2022.
- [7] X. Sun, H. Xu, J. Dong, H. Zhou, C. Chen, and Q. Li, "Few-shot learning for domain-specific fine-grained image classification," *IEEE Transactions on Industrial Electronics*, vol. 68, no. 4, pp. 3588–3598, 2021.
- [8] O. Vinyals, C. Blundell, T. Lillicrap, K. Kavukcuoglu, and D. Wierstra, "Matching networks for one shot learning," in *Proceedings of Advances in Neural Information Processing Systems (NIPS) 2016*, vol. 29, 2016, pp. 3637–3645.
- [9] H. Chen, H. Li, Y. Li, and C. Chen, "Multi-scale adaptive task attention network for few-shot learning," *Arxiv Preprint Arxiv:2011.14479*, 2020.
- [10] X.-S. Wei, P. Wang, L. Liu, C. Shen, and J. Wu, "Piecewise classifier mappings: learning fine-grained learners for novel categories with few examples," *IEEE Transactions on Image Processing*, vol. 28, no. 12, pp. 6116–6125, 2019.
- [11] W. Li, J. Xu, J. Huo, L. Wang, Y. Gao, and J. Luo, "Distribution consistency based covariance metric networks for few-shot learning," in *Proceedings of The AAAI Conference on Artificial Intelligence*, vol. 33, no. 1, 2019, pp. 8642–8649.
- [12] Y. Zhu, C. Liu, and S. Jiang, "Multi-attention meta learning for few-shot fine-grained image recognition," in *Proceedings of International Joint Conference on Artificial Intelligence*, 2020, pp. 1090–1096.
- [13] H. Huang, J. Zhang, J. Zhang, Q. Wu, and J. Xu, "Compare more nuanced: pairwise alignment bilinear network for few-shot fine-grained learning," in *Proceedings of IEEE International Conference on Multimedia and Expo (ICME)*, 2019, pp. 91–96.
- [14] H. Huang, J. Zhang, J. Zhang, J. Xu, and Q. Wu, "Low-rank pairwise alignment bilinear network for few-shot fine-grained image classification," *IEEE Transactions on Multimedia*, vol. 23, pp. 1666–1680, 2021.
- [15] J. Snell, K. Swersky, and R. Zemel, "Prototypical networks for few-shot learning," in *Proceedings of International Conference on Neural Information Processing Systems (NIPS) 17*, vol. 30, 2017, p. 4080–4090.
- [16] H. Zhang, H. Li, and P. Koniusz, "Multi-level second-order few-shot learning," *IEEE Transactions on Multimedia*, 2022.
- [17] C. Finn, P. Abbeel, and S. Levine, "Model-agnostic meta-learning for fast adaptation of deep networks," in *Proceedings of the 34th International Conference on Machine Learning*, vol. 70, 2017, pp. 1126–1135.
- [18] X. Zhong, C. Gu, M. Ye, W. Huang, and C.-W. Lin, "Graph complemented latent representation for few-shot image classification," *IEEE Transactions on Multimedia*, 2022.
- [19] S. Yang, L. Liu, and M. Xu, "Free lunch for few-shot learning: distribution calibration," in *Proceedings of International Conference on Learning Representations*, 2021.
- [20] N. Zhang, J. Donahue, R. Girshick, and T. Darrell, "Part-based R-CNNs for fine-grained category detection," in *Proceedings of European Conference on Computer Vision*, 2014, pp. 834–849.
- [21] Y. Zhang, X.-S. Wei, J. Wu, J. Cai, J. Lu, V.-A. Nguyen, and M. N. Do, "Weakly supervised fine-grained categorization with part-based image representation," *IEEE Transactions on Image Processing*, vol. 25, no. 4, pp. 1713–1725, 2016.
- [22] L. Zhang, S. Huang, W. Liu, and D. Tao, "Learning a mixture of granularity-specific experts for fine-grained categorization," in *Proceedings of The IEEE/CVF International Conference on Computer Vision*, 2019, pp. 8331–8340.
- [23] K. Song, X.-S. Wei, X. Shu, R.-J. Song, and J. Lu, "Bi-modal progressive mask attention for fine-grained recognition," *IEEE Transactions on Image Processing*, vol. 29, pp. 7006–7018, 2020.
- [24] S. Feng, "Kernel pooling feature representation of pre-trained convolutional neural networks for leaf recognition," *Multimedia Tools and Applications*, vol. 81, no. 3, pp. 4255–4282, 2022.
- [25] C. Wang, S. Song, Q. Yang, X. Li, and G. Huang, "Fine-grained few shot learning with foreground object transformation," *Neurocomputing*, vol. 466, pp. 16–26, 2021.
- [26] X. Ruan, G. Lin, C. Long, and S. Lu, "Few-shot fine-grained classification with spatial attentive comparison," *Knowledge-based Systems*, vol. 218, p. 106840, 2021.
- [27] M. Ehrlich and L. S. Davis, "Deep residual learning in the JPEG transform domain," in *Proceedings of The IEEE/CVF International Conference on Computer Vision*, 2019, pp. 3484–3493.
- [28] J. Wang, S. Chen, Z. Wu, and Y.-G. Jiang, "FT-TDR: frequency-guided transformer and top-down refinement network for blind face inpainting," *IEEE Transactions on Multimedia*, 2022.
- [29] K. Xu, M. Qin, F. Sun, Y. Wang, Y.-K. Chen, and F. Ren, "Learning in the frequency domain," in *Proceedings of The IEEE/CVF Conference on Computer Vision and Pattern Recognition*, 2020, pp. 1740–1749.
- [30] Z. Qin, P. Zhang, F. Wu, and X. Li, "FcaNet: frequency channel attention networks," in *Proceedings of The IEEE/CVF International Conference on Computer Vision*, 2021, pp. 783–792.
- [31] H.-J. Ye, H. Hu, D.-C. Zhan, and F. Sha, "Few-shot learning via embedding adaptation with set-to-set functions," in *Proceedings of the IEEE/CVF Conference on Computer Vision and Pattern Recognition*, 2020, pp. 8808–8817.
- [32] A. Khosla, N. Jayadevaprakash, B. Yao, and F.-F. Li, "Novel dataset for fine-grained image categorization: Stanford dogs," in *Proceedings of*

first Workshop on Fine-Grained Visual Categorization, IEEE Conference on Computer Vision and Pattern Recognition, 2011.

- [33] K. Jonathan, S. Michael, D. Jia, and F.-F. Li, "3D object representations for fine-grained categorization," in *Proceedings of The IEEE International Conference on Computer Vision Workshops*, 2013, pp. 554–561.
- [34] O. Russakovsky, J. Deng, H. Su, J. Krause, S. Satheesh, S. Ma, Z. Huang, A. Karpathy, A. Khosla, M. Bernstein, A. C. Berg, and L. Fei-Fei, "Imagenet large scale visual recognition challenge," *International Journal of Computer Vision*, vol. 115, no. 3, pp. 211–252, 2015.
- [35] X. Li, J. Wu, Z. Sun, Z. Ma, J. Cao, and J.-H. Xue, "BSNet: bi-similarity network for few-shot fine-grained image classification," *IEEE Transactions on Image Processing*, vol. 30, pp. 1318–1331, 2020.
- [36] F. Sung, Y. Yang, L. Zhang, T. Xiang, P. H. Torr, and T. M. Hospedales, "Learning to compare: relation network for few-shot learning," in *Proceedings of The IEEE Conference on Computer Vision and Pattern Recognition*, 2018, pp. 1199–1208.
- [37] V. Garcia and J. Bruna, "Few-shot learning with graph neural networks," in *Proceedings of International Conference on Learning Representations*, 2018.
- [38] W. Li, L. Wang, J. Xu, J. Huo, Y. Gao, and J. Luo, "Revisiting local descriptor based image-to-class measure for few-shot learning," in *Proceedings of The IEEE/CVF Conference on Computer Vision and Pattern Recognition*, 2019, pp. 7260–7268.
- [39] C. Dong, W. Li, J. Huo, Z. Gu, and Y. Gao, "Learning task-aware local representations for few-shot learning," in *Proceedings of The Twenty-ninth International Conference on International Joint Conferences on Artificial Intelligence*, 2021, pp. 716–722.
- [40] H. Huang, J. Zhang, L. Yu, J. Zhang, Q. Wu, and C. Xu, "TOAN: target-oriented alignment network for fine-grained image categorization with few labeled samples," *IEEE Transactions on Circuits and Systems for Video Technology*, vol. 32, no. 2, pp. 853–866, 2022.
- [41] S. Cao, W. Wang, J. Zhang, M. Zheng, and Q. Li, "A few-shot fine-grained image classification method leveraging global and local structures," *International Journal of Machine Learning and Cybernetics*, vol. 13, pp. 2273–2281, 2022.
- [42] W. Zhang, X. Liu, Z. Xue, Y. Gao, and C. Sun, "NdpNet: a novel non-linear data projection network for few-shot fine-grained image classification," *Arxiv Preprint Arxiv:2106.06988*, 2021.
- [43] H. Chen, H. Li, Y. Li, and C. Chen, "Multi-level metric learning for few-shot image recognition," *Arxiv Preprint Arxiv:2103.11383*, 2021.
- [44] W.-Y. Chen, Y.-C. Liu, Z. Kira, Y.-C. F. Wang, and J.-B. Huang, "A closer look at few-shot classification," in *Proceedings of International Conference on Learning Representations*, 2019.
- [45] R. Hou, H. Chang, B. Ma, S. Shan, and X. Chen, "Cross attention network for few-shot classification," in *Proceedings of Advances in Neural Information Processing Systems (NIPS' 2019)*, vol. 32, 2019, pp. 4003–4014.
- [46] C. Zhang, Y. Cai, G. Lin, and C. Shen, "Deepemd: few-shot image classification with differentiable earth mover's distance and structured classifiers," in *Proceedings of The IEEE/CVF Conference on Computer Vision and Pattern Recognition*, 2020, pp. 12 203–12 213.
- [47] Y. Tian, Y. Wang, D. Krishnan, J. B. Tenenbaum, and P. Isola, "Rethinking few-shot image classification: a good embedding is all you need?" in *Proceedings of European Conference on Computer Vision*, 2020, pp. 266–282.
- [48] B. Liu, Y. Cao, Y. Lin, Q. Li, Z. Zhang, M. Long, and H. Hu, "Negative margin matters: understanding margin in few-shot classification," in *Proceedings of European Conference on Computer Vision*, 2020, pp. 438–455.
- [49] C. Liu, Y. Fu, C. Xu, S. Yang, J. Li, C. Wang, and L. Zhang, "Learning a few-shot embedding model with contrastive learning," in *Proceedings of the AAAI Conference on Artificial Intelligence*, vol. 35, 2021, pp. 8635–8643.
- [50] D. Kang, H. Kwon, J. Min, and M. Cho, "Relational embedding for few-shot classification," in *Proceedings of The IEEE/CVF International Conference on Computer Vision*, 2021, pp. 8822–8833.
- [51] A. Afrasiyabi, J.-F. Lalonde, and C. Gagné, "Mixture-based feature space learning for few-shot image classification," in *Proceedings of The IEEE/CVF International Conference on Computer Vision*, 2021, pp. 9041–9051.
- [52] S. Qiao, C. Liu, W. Shen, and A. L. Yuille, "Few-shot image recognition by predicting parameters from activations," in *Proceedings of the IEEE Conference on Computer Vision and Pattern Recognition*, 2018, pp. 7229–7238.
- [53] Z. Chen, J. Ge, H. Zhan, S. Huang, and D. Wang, "Pareto self-supervised training for few-shot learning," in *Proceedings of The IEEE/CVF Conference on Computer Vision and Pattern Recognition*, 2021, pp. 13 663–13 672.
- [54] S. Gidaris and N. Komodakis, "Generating classification weights with GNN denoising autoencoders for few-shot learning," in *Proceedings of the IEEE/CVF Conference on Computer Vision and Pattern Recognition*, 2019, pp. 21–30.
- [55] P. Mangla, N. Kumari, A. Sinha, M. Singh, B. Krishnamurthy, and V. N. Balasubramanian, "Charting the right manifold: manifold mixup for few-shot learning," in *Proceedings of the IEEE/CVF Winter Conference on Applications of Computer Vision*, 2020, pp. 2218–2227.
- [56] Y. Lifchitz, Y. Avrithis, S. Picard, and A. Bursuc, "Dense classification and implanting for few-shot learning," in *Proceedings of The IEEE/CVF Conference on Computer Vision and Pattern Recognition*, 2019, pp. 9258–9267.
- [57] S. Huang, Q. Wang, S. Zhang, S. Yan, and X. He, "Dynamic context correspondence network for semantic alignment," in *Proceedings of the IEEE/CVF International Conference on Computer Vision*, 2019, pp. 2010–2019.



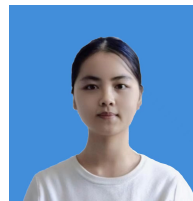
Hegui Zhu received the B.S. degree in information and computation science and the M.S. degree in applied mathematics from Northeastern University, Shenyang, China, in 2003 and 2006, respectively, and the Ph.D. degree in operational research and cybernetics from Jilin University, Changchun, China, in 2014. He is currently an Associate Professor with the Department of Mathematics, College of Sciences, Northeastern University. His current research interests include machine learning, image processing, and multimedia security.



Zhan Gao received the B.S. degree from the School of mathematics and Information Science, Henan Normal University, Xinxiang, China, in 2020. She is currently working toward the M.S. degree at Northeastern University, Shenyang, China. Her research interests include deep learning, and image classification.



Jiayi Wang received the B.S. degree in information and computation sciences from Northeastern University, Shenyang, China, in 2020, where she is currently pursuing the M.S. degree in applied mathematics. Her research interest includes data mining, machine learning, deep learning, and big data analysis.



Yange Zhou received the B.S. degree in information and computation science, Northeastern University, Shenyang, China, in 2021. She is currently working toward the M.S. degree at Northeastern University, Shenyang, China. Her research interests include deep learning and computer vision.



Chengqing Li received his M.Sc. degree in Applied Mathematics from Zhejiang University, China in 2005 and his Ph.D. degree in Electronic Engineering from City University of Hong Kong in 2008. Thereafter, he worked as a Postdoctoral Fellow at The Hong Kong Polytechnic University till September 2010. From April 2013 to July 2014, he worked at the University of Konstanz, Germany, under the support of the Alexander von Humboldt Foundation. Now, he is working at School of Computer Science, Xiangtan University, China as the dean. Prof. Li

focuses on security analysis of multimedia encryption schemes and privacy protection schemes. He has published about sixty papers on the subject in the past 18 years, receiving more than 4800 citations with h-index 37.